Postcollision interaction effects in KLL Auger spectra following argon 1s photoionization

R. Guillemin,[1,2] S. Sheinerman,[3] R. Püttner,[4] T. Marchenko,[1,2] G. Goldsztejn,[1,2] L. Journel,[1,2] R. K. Kushawaha,[1,2] D. Céolin,[5] M. N. Piancastelli,[1,2,6] and M. Simon[1,2,5]

[1]*Sorbonne Universités, UPMC Université Paris 06, UMR 7614, Laboratoire de Chimie Physique Matière et Rayonnement, F-75005 Paris, France*

[2]*CNRS, UMR 7614, Laboratoire de Chimie Physique Matière et Rayonnement, F-75005 Paris, France*

[3]*Department of Physics, St. Petersburg State Maritime Technical University, 198262 St. Petersburg, Russia*

[4]*Institut für Experimentalphysik, Freie Universität Berlin, Arnimallee 14, D-14195 Berlin, Germany*

[5]*Synchrotron SOLEIL, l'Orme des Merisiers, Saint-Aubin, Boîte Postale 48, 91192 Gif-sur-Yvette Cedex, France*

[6]*Department of Physics and Astronomy, Uppsala University, P.O. Box 516, SE-751 20 Uppsala, Sweden*

(Received 15 April 2015; published 6 July 2015)

Postcollision interaction effects on the Auger decay of a deep core hole are studied both experimentally and theoretically. $KL_{2,3}L_{2,3}$ decay spectra of the Ar 1s vacancy are measured with high-energy resolution with excess photon energies ranging from 0 to 200 eV above the ionization threshold. Interaction of the Auger electron with the photoelectron and the ion field manifests itself in the Auger spectra as a distortion of the energy distribution of the Auger electron close to threshold. Moreover, recapture of the photoelectron due to energy exchange is dominating in the low-photon-energy range above threshold. The experimental results are compared with calculations based on the semiclassical approach to the postcollision interaction. The energies of the discrete levels and individual recapture cross sections are computed in the Hartree-Fock approximation. Good agreement is found between the calculated and experimental spectra, validating the model used.

DOI: 10.1103/PhysRevA.92.012503 PACS number(s): 31.15.xg, 32.70.Jz, 32.80.Aa, 32.80.Hd

I. INTRODUCTION

Auger spectroscopy following deep atomic-shell ionization is a powerful probe of electron correlations in atoms. The investigation of near-threshold photoionization of an inner atomic shell, followed by the emission of one or several Auger electrons, is of particular interest. In this case, a slow photoelectron leaving the atom interacts strongly with the ionic field, which varies during the vacancy decay, as well as with the Auger electrons. Such an interaction, which is known as a postcollision interaction (PCI), has been widely investigated over the course of several decades (see, e.g., reviews [1,2]). PCI leads to a noticeable modification of the photoelectron and Auger electron spectra: the electron lines are shifted in energy and their shapes are distorted. The slow photoelectron loses energy due to PCI, and the velocity of the fast Auger electron increases. PCI distortion depends on several characteristics of the inner vacancy and on the kinematics of the emitted electrons, namely on the natural width Γ of the inner hole and the final state of the Auger decay as well as on the kinetic energies and emission angles of the photoelectron and Auger electron. Thus, the investigation of PCI effects in electron spectra allows one to obtain information on the widths and energies of the inner and intermediate atomic shells [3].

Experimentally, the systematic investigation of PCI effects was carried out mainly on the spectra of slow photoelectrons. Multielectron coincidence spectroscopy [4,5] allows one to reliably select a decay pathway and ascribe it to the recorded photoelectron spectrum. Using this technique, PCI distortion of photoelectron spectra has been investigated for single Auger (SA) decay of Ar 2p, Kr 3d, and Xe 4d vacancies [6–8], as well as for double Auger (DA) decay of Ar 2p, Ar 2s, and Kr 3d vacancies [6,9,10]. However, the multielectron coincidence method is not very efficient for large kinetic energy differences between photoelectrons and Auger electrons, and thus it cannot be applied to the decay of deep inner vacancies. In this case, another technique, namely slow photoelectron-selected ion coincidences, has allowed the observation of PCI distortion of photoelectrons associated with SA, DA, and multiple Auger (MA) decays of the inner shell vacancy. Such an approach was applied to the decays of the Ar 1s vacancy [3] and the S 1s vacancy in carbonyl sulfide (OCS) [11].

In the near-threshold region, the effect of PCI on fast Auger electrons has been investigated by high-resolution electron spectra measurements for the decay of Xe 4d [12] and Ne 1s [13] vacancies. These authors showed that in the region just above the ionization threshold, where the excess energy is less than twice the lifetime width of the inner vacancy, the Auger spectra are dominated by the recapture of the slow photoelectron into Rydberg states of the singly charged atomic ion. Photoelectron recapture in the near-threshold region has also been studied through high-energy electron spectroscopy in N_2 [14] and H_2O [15].

In this work, we investigate the energy distribution of Auger electrons following deep-inner-vacancy decay in Ar. Creation of a vacancy in outer or intermediate shells is followed mainly by SA decay, as seen in the decays of $L_{2,3}$ vacancies in Ar [16–18] and of the N_5 vacancy in Xe [19]. In contrast, the dynamics of deep-vacancy decay can be rather complicated [20,21] and includes DA and MA decays, which occur through the creation and decay of intermediate quasistationary states. However, because of the large energy difference between inner atomic shells, the energy of the Auger electron emitted in the first step of the deep-vacancy decay is large and well separated from the energies of other emitted electrons. The first Auger electron leaves the reaction zone very quickly, and the subsequent decay of the intermediate hole states does not contribute essentially to the PCI distortion of the Auger line shapes.

Our measurements show a strong PCI distortion of the Auger electron line shape that depends on the incident photon

energy, and it is modeled by the calculation in the semiclassical approximation. Apart from the shift and asymmetrical shape of the line, the PCI capture of the slow photoelectron into the discrete Rydberg states of the Ar^+ ions is observed at small excess energies of the incident photon above the $1s$ threshold. Quantum-mechanical calculations that include both the continuum part of the Auger spectrum and the individual recapture probabilities as a function of excess energy allow us to reproduce the complete decay spectrum at photon energies close to threshold. The calculation results show good agreement with the experimental Auger spectra measured with high resolution.

Our paper is organized as follows: In Sec. II, we give a short description of the decay process and theoretical approach used in this study. In Sec. III, we describe the experimental setup used to measure the Auger spectra presented in the paper. In Sec. IV, we present and discuss the results, focusing on how PCI affects the shape and energy position of the Auger lines in Sec. IV A, and on low excess energy recapture to discrete states in Sec. IV B. Finally, we give a short conclusion of this study in Sec. V.

II. DESCRIPTION OF PCI DISTORTION OF AUGER LINES

When Ar $1s$ photoionization is followed by KLL Auger emission, one can write the decay scheme as

$$\gamma + \mathrm{Ar} \rightarrow \mathrm{Ar}^+(1s^{-1}) + e^-_{\mathrm{ph}} \rightarrow \mathrm{Ar}^{2+}(2p^{-2}) + e^-_{\mathrm{ph}} + e^-_{KLL} \rightarrow \cdots \rightarrow \mathrm{Ar}^{(n+2)+} + e^-_{\mathrm{ph}} + e^-_{KLL} + \cdots + e^-_n. \quad (1)$$

Here e^-_{ph} is the photoelectron and e^-_{KLL} is the KLL Auger electron emitted during the decay of the $1s$ vacancy, and we consider the Auger processes that occur through the creation and decay of the intermediate $\mathrm{Ar}^{2+}(2p^{-2})$ state. Dots reflect the following decay of the intermediate $(2p^{-2})$ state to the final ionic state $\mathrm{Ar}^{(n+2)+}$ with the emission of n additional e^-_n Auger electrons. Note that there are different decay pathways, and their dynamics can be rather complicated with the emission of two or more additional Auger electrons. The direct or cascade Auger decay of the $2p^{-2}$ intermediate state with the emission of a few Auger electrons influences the energy distribution of the photoelectron, i.e., it contributes to the PCI distortion of the photoelectron line, as was demonstrated recently [3]. Here, we focus on the $KL_{2,3}L_{2,3}$ Auger spectrum at large kinetic energy, $E_{KLL} \sim 2650$ eV. The e^-_{KLL} electron leaves the reaction zone quickly and is only slightly affected by the subsequent Auger decays. This means that the energy exchange between the first Auger electron and the photoelectron occurs due to the first Auger decay solely, and the PCI distorted energy distribution of the fast KLL Auger electron is close to the one recorded in the single Auger decay process. This is true if the lifetimes of the intermediate $(2p^{-2})$ states are large and the emitted $KL_{2,3}L_{2,3}$ Auger electron travels a large distance when the decay of the $\mathrm{Ar}^{2+}(2p^{-2})$ states occurs.

According to the width of these states, $\Gamma \sim 250$ meV [22], this distance can be estimated at 1500 a.u. In this case, the $KL_{2,3}L_{2,3}$ Auger electron is only slightly affected by the subsequent Auger decays. Note that other intermediate states $(2s^{-2}$ or $2s^{-1}2p^{-1})$ have shorter lifetimes, thus the emitted KLL Auger electrons are located much closer to the atom and can be influenced notably by the subsequent Auger decays.

Therefore, computation approaches developed for the description of PCI in single Auger decays can be applied to the calculation of PCI effects in the spectrum of $KL_{2,3}L_{2,3}$ Auger electrons emitted in process (1). In this case, PCI reduces to the interaction of the photoelectron with the ionic field, which varies during the SA decay and the interaction between the photoelectron and the first Auger electron. There are a number of approaches to describe PCI effects in SA decay following inner-shell photoionization, namely classical, semiclassical, and quantum-mechanical approaches [23–32]. The focus of our study is PCI distortion for small excess energies of incident photons above the inner-shell threshold. Hence, for calculation of the PCI-affected photoionization cross section, we have used the semiclassical approach, which is valid for low photoelectron energies. The expressions for the cross section and amplitude of this process have been presented in previous works [31,33]. These expressions depend on the relative angle between the photoelectron and Auger electron emission directions. The angle-dependent PCI distortion cross sections have been investigated earlier both theoretically [27,30,31,33,34] and experimentally [35–38]. It should be noted that angle-dependent PCI distortion manifests itself in measurements where the emitted photoelectron and Auger electron are recorded in coincidence. In our study, we performed noncoincident measurements in which only the Auger electron is measured. Hence, for a correct description of the experimental results, the angular-dependent cross sections obtained within the semiclassical approach have to be integrated over all possible relative angles of the photoelectron and Auger electron emission. Our calculations being based on the semiclassical approach, an isotropic distribution of the photoelectron is assumed. Although $1s$ photoelectrons are anisotropic (the anisotropy parameter β has a fixed value of 2 in a nonrelativistic treatment), both anisotropic and isotropic distributions give the same line shapes in semiclassical calculations for noncoincident experiments, i.e., after integration over all possible relative angles [31,33,34].

PCI distortion naturally depends on the width Γ of the $1s$ vacancy. Literature values for the width of the $1s$ vacancy vary from 650 to 700 meV [39–42]. In this study, we found a better general agreement between the calculated and the experimental spectra using the lower value 650 meV [40]. It should be noted that the approximation of the real process (1) by SA decay implies that the $\mathrm{Ar}^{2+}(2p^{-2})$ final ionic states have a finite lifetime τ_f leading to a spread in energy following a Lorentzian distribution with width $\Gamma_f = 1/\tau_f$. Hence, the energy of the emitted $KL_{2,3}L_{2,3}$ Auger electron, independently of the PCI influence, must also be affected by this energy distribution, and the correct description of the Auger spectrum demands an additional convolution of the calculated PCI distorted Auger spectrum with a Lorentzian of width Γ_f [43–45]. In this study, the value of Γ_f was chosen to be 236 meV, which is twice the 118 meV width of the $2p^{-1}$ single core-hole state [46], and it is in line with high-resolution measurement of the resonant Auger decay in argon [22].

III. EXPERIMENT

The experimental measurements were carried out at the French national synchrotron facility SOLEIL, GALAXIES beamline [47], on the new HAXPES end station dedicated to hard-x-ray photoelectron spectroscopy [22,48–50]. Linearly polarized light is provided by a U20 undulator and monochromatized by a Si(111) double-crystal. Electrons are analyzed by a large acceptance angle EW4000 Scienta hemispherical analyzer, which lens axis is set parallel to the polarization. The experimental resolutions were carefully estimated from Ne 1s photoelectrons and Auger electrons measurements. The photon bandwidth δE delivered by the beamline is 350 meV at 3200 eV photon energy. Two sets of data were recorded. The low excess energy data set, from 0 to 5 eV above threshold, was recorded at an estimated experimental resolution of 300 meV and includes the electron spectrometer resolution (280 meV) and the Doppler broadening (100 meV at room temperature for electrons with 2.66 keV kinetic energy [51]). The high-energy data set, from 5 to 180 eV, was recorded with a spectrometer resolution of 490 meV, including the Doppler broadening. In this study, the normal Auger spectrum is measured above the 1s ionization threshold (3206.3 eV [52]). Calibration of the photon energy was made on the $1s \rightarrow 4p$ transition at 3203.54 eV [53]. Measurements were taken in the 2650–2675 eV electron kinetic energy range with 0.1 eV steps while varying the photon energy from 3201 eV, i.e., 5 eV below the ionization threshold, up to 3395 eV.

We show in Fig. 1 the experimental two-dimensional (2D) map recorded in the photon energy range 3201–3209 eV to give an overview of the Auger lines around the ionization threshold. One remarkable feature of the Auger emission in Fig. 1 is that the normal Auger peaks, $KL_{2,3}L_{2,3}(^1D_2)$ and $(^1S_0)$ [54], show decreasing kinetic energies with increasing photon energy above threshold. This is interpreted as evidence of the energy exchange between the KLL Auger electron and the photoelectron. In the following, individual Auger spectra are analyzed and we focus on the main $^1D_2$ line of the $KL_{2,3}L_{2,3}$ Auger spectrum. Note that the second weaker Auger line, $^1S_0$, shows exactly the same behavior. The second remarkable feature is the smooth transition from below threshold into the ionization continuum with the extension of the Rydberg series above threshold, linearly dispersing with photon energy. In the following, we tentatively conduct theoretical calculations to describe these two features.

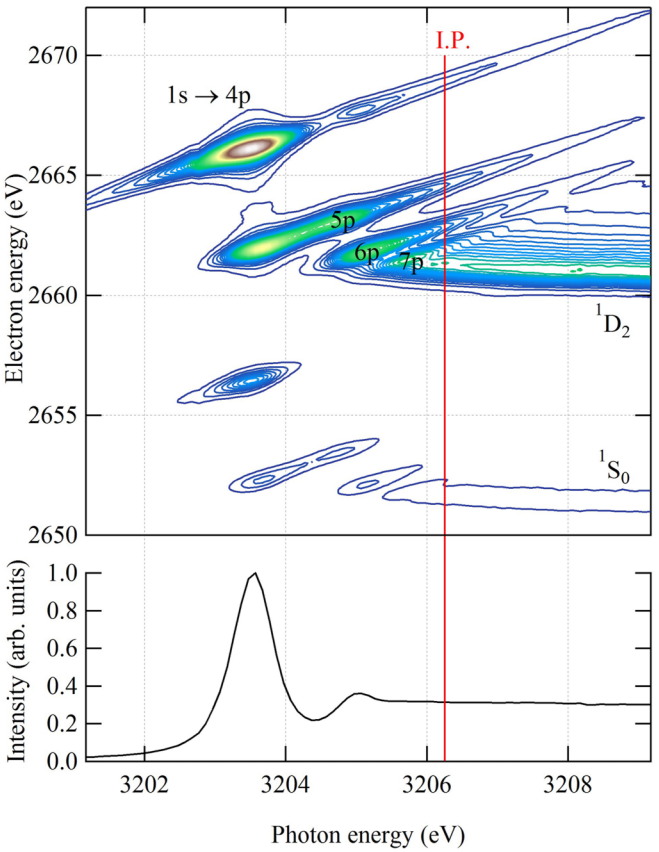

FIG. 1. (Color online) (Top) $KL_{2,3}L_{2,3}$ Auger relaxation of 1s core excited argon represented as a 2D map showing the Auger electron energy as a function of incident photon energy. The different excitations to discrete electronic states are indicated below threshold and final ionized states above. (Bottom) Absorption spectrum of Ar around the 1s ionization threshold, I.P., indicated as a vertical solid line.

IV. RESULTS OF MEASUREMENTS AND CALCULATIONS

A. Energy shift and line shape

The results of measurements and calculations of the Auger lines $KL_{2,3}L_{2,3}(^1D_2)$ for excess energies $E_{\rm exc}$ of 1, 2.5, 5, 10, 20, and 100 eV above threshold are presented in Fig. 2. The calculations have been carried out on the basis of the semiclassical approach. We used 2660.8 eV for the unshifted value of the Auger electron energy (see below).

To compare with the measurements, the theoretical line shapes were convoluted with a Lorentzian of 236 meV full width at half-maximum (FWHM) that simulates the spread of the $Ar^{2+}(2p^{-2})$ state energy and with a Gaussian of 300 meV FWHM that simulates the total experimental resolution function for excess energies below 5 eV, and a FWHM of 490 meV above 5 eV. The calculated curves in Fig. 2 have been shifted by values ranging from 100 to 200 meV to match the energy position of the experimental curves. Such a disagreement between the measured and calculated line shapes can be associated with some uncertainties in the experimental calibration of the energy scale for different energies of the incident photons. The good general agreement between the measured and calculated shapes shows that the parameters of calculation are rather reliable, and the model used describes adequately the experimental results. Both the measurements and the calculation show the strong PCI influence on the Auger electron line shape. The lower the excess photon energy above the 1s threshold, the larger is the shift of the energy distribution maximum and the asymmetry of the line shape.

From the experimental measurements, the value for unshifted energy of the $^1D_2$ Auger line is found to be 2660.8 eV, as a limit of location of the line-shape maximum at large excess photon energy over the threshold (150 eV). Theoretical results using this value as a parameter of calculation show very good agreement with the measured line shapes both for small and large excess photon energies. Using this value of the unshifted Auger line and the energy of the 1s vacancy in the $Ar^+(1s^{-1})$ ion, 3206.3 eV [52], we can estimate the energy

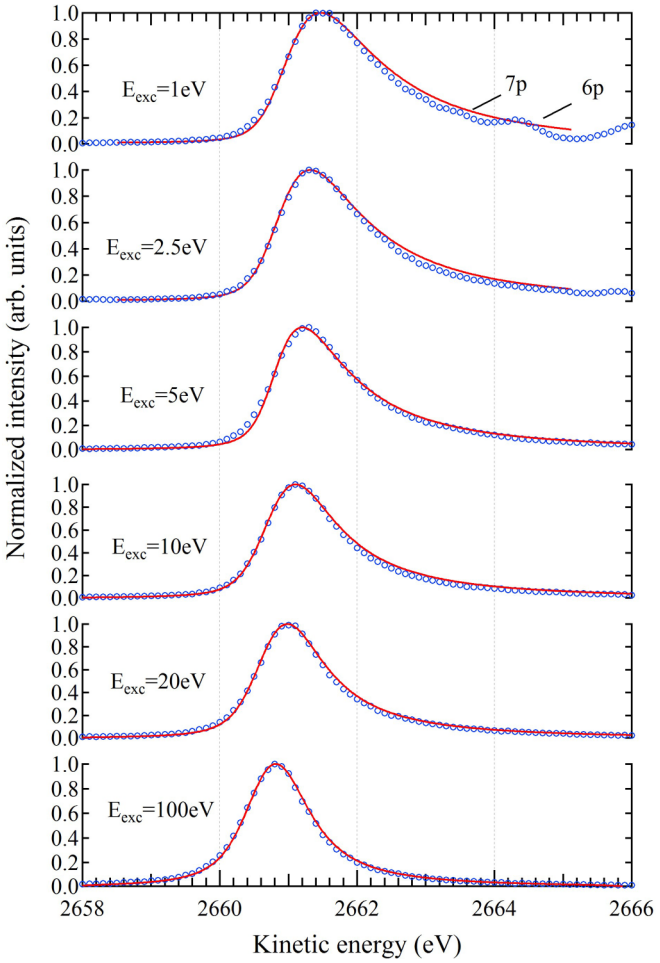

FIG. 2. (Color online) Measured (blue circles) and calculated (red lines) $KL_{2,3}L_{2,3}(^1D_2)$ Auger line profiles for selected excess energies ($E_{\rm exc}$) above the Ar 1s ionization threshold.

of the intermediate state with two vacancies in the $2p$ shell: $E[2p^{-2}(^1D_2)] = 545.5$ eV.

In Fig. 3, we show the measured and calculated dependence of the line shift $\Delta\epsilon$ on the excess energy $E_{\rm exc}$ above threshold for the $^1D_2$ transition. The energy shift is given relative

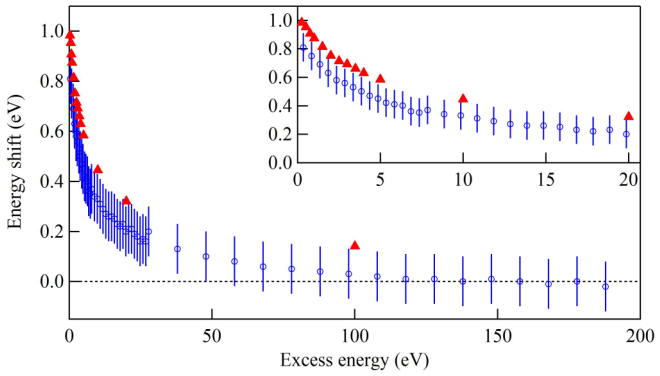

FIG. 3. (Color online) Measured (blue circles with error bars) and calculated (red triangles) line shift $\Delta\epsilon$ as a function of excess energy $E_{\rm exc}$ above the ionization threshold for the $KL_{2,3}L_{2,3}(^1D_2)$ Auger line.

to the unshifted value 2660.8 eV measured at high photon energies above threshold, i.e., between 120 and 190 eV of excess energy. As a result of the findings presented in Fig. 3, close to threshold the photon bandwidth δE has—at least in principle—an influence on the Auger spectrum. As displayed in the figure, directly above threshold the line shift $\Delta\epsilon$ of the Auger electron depends strongly on the photon energy, i.e., the line shift varies over the photon bandwidth δE. This variation can be estimated by $\delta\Delta\epsilon = \frac{d(\Delta\epsilon)}{dE_{exc}}\delta E$. In the present case, $\delta E = 350$ meV, resulting in $\delta\Delta\epsilon \cong 105$ meV directly above threshold. This value drops rapidly with increasing $E_{\rm exc}$, and the resulting peak broadening is insignificant for the present analysis, however it may become important in other cases, particularly for larger photon bandwidths.

For the entire region, a good agreement of the measured and calculated values is found, although at small excess photon energies $E_{\rm exc} \leqslant 1$ eV the calculated shift is slightly larger than the measured one. The results of measurements and calculations presented in Figs. 2 and 3 confirm the reliability of the Auger decay parameters, the width of the 1s vacancy, $\Gamma = 650$ meV, and the unshifted energy of the $KL_{2,3}L_{2,3}(^1D_2)$ Auger electron, $E_A^{(0)} = 2660.8$ eV.

B. Recapture to discrete states

Similar to the observations made on the near-threshold Xe 4d [12] and Ne 1s [13] decay spectra, the Ar 1s Auger spectrum measured at 1 eV in Fig. 2 shows oscillating structures lying on the large-energy wing of the Auger line shape. The same structures are observed in our measurements at other near-threshold photon energies. From the 2D map in Fig. 1 it is clear that these structures correspond to the resonant Auger decay of the Rydberg series $4p$, $5p$, $6p$, and $7p$ that extends over the threshold region. The energy positions of these resonant Auger electrons follow a linear dispersion with photon energy below and above threshold. The extension of the resonant Auger decay from the Rydberg series above threshold corresponds to PCI recapture of the slow photoelectron into the discrete states of the doubly charged ion, and it can be interpreted in semiclassical language as a shakedown process. The positions of the maxima of these structures have to correspond to the energies of the discrete states in the field of the doubly charged ion. From the conservation law

$$E_{\rm ph}^{(0)} + E_{\rm Aug}^{(0)} = E_{\rm ph} + E_{\rm Aug}, \tag{2}$$

with $E_{\rm ph}$ and $E_{\rm Aug}$ being the energies of the photoelectron and Auger electron in the final states, respectively, as well as $E_{\rm ph}^{(0)}$ and $E_{\rm Aug}^{(0)}$ being the corresponding unshifted values, it follows that

$$E_{\rm ph} = E_{\rm ph}^{(0)} + E_{\rm Aug}^{(0)} - E_{\rm Aug} = E_{\rm ph}^{(0)} - \Delta E. \tag{3}$$

Here $E_{\rm ph}^{(0)} = E_{\rm exc}$ is the excess photon energy over the 1s threshold, and $\Delta E = E_{\rm Aug} - E_{\rm Aug}^{(0)}$ is the exchange of energy between the photoelectron and the Auger. Due to PCI, the slow photoelectron loses energy and the fast Auger electron gains energy. If the energy exchange ΔE is more than the unshifted value of the slow photoelectron $E_{\rm ph}^{(0)}$, $E_{\rm ph}$ has a negative value, i.e., the photoelectron is recaptured into a discrete state. Thus,

we can estimate the energy position of the discrete states using Eq. (3).

To confirm this observation, we have calculated in the Hartree-Fock (HF) approximation the energies of the discrete levels $1s^2 2s^2 2p^4 3s^2 3p^6 np$ ($n = 4$–15) of the Ar^+ ion by using the value averaged over the different terms of the corresponding configuration. The results of the calculations of the discrete states show a rather good agreement with the measured values estimated on the basis of Eq. (3).

We have calculated also the relative probabilities, $P_{\rm dis}^{(n)}$, of the PCI recapture into the discrete states for $n = 4$–15 using a quantum-mechanical PCI model [25,55] that takes into account the interaction of the slow photoelectron with the ion field, which varies during Auger decay. The amplitude of a process in this approach is proportional to the overlap integral between the function $A(E_{\rm exc})$, which describes the emission of an electron from the inner shell and its propagation with the complex energy $E_{\rm exc} + i\,\Gamma/2$ in the field of the singly charged ion followed by the Auger decay, and the photoelectron wave function in the final state, i.e., after the Auger decay. The final state is either in the continuum or a discrete state in the case of electron recapture. The square of the modulus of the function $A(E_{\rm exc})$ determines the total cross section, $\sigma_{\rm tot}(E_{\rm exc})$, for the absorption of the photon by the inner shell, followed by Auger decay [56]. Note that in this work, we are interested in the Auger electron line shape solely, hence we have not calculated the matrix elements of the Auger decay, and we have obtained the relative probabilities $P_{\rm dis}^{(n)}$ in arbitrary units.

Figure 4(a) shows the experimental spectrum measured at excess energy $E_{\rm exc} = 1$ eV together with a tentative fit to the individual discrete state contributions. The calculated Auger electron energy distribution, including both the continuum part and the recapture to discrete np states with $n = 4$–15, is shown in Fig. 4(b). Figure 4(c) compares the calculated spectrum with the experimental one.

To calculate the Auger electron energy distribution in the region of photoelectron recapture, we have simulated the shapes of the discrete states by the Lorentzian

$$\frac{d\sigma}{d\varepsilon} = \frac{\sigma_0}{\varepsilon^2 + \Gamma_{\rm dis}^2/4}, \tag{4}$$

where $\Gamma_{\rm dis}$= 236 meV is the estimated lifetime of the $2p^{-2}$ states (see above). The reason to take this value for $\Gamma_{\rm dis}$ is that when the photoelectron is overtaken by the Auger electron, the decay of the $1s^{-1}$ has already happened and the photoelectron now interacts with a $2p^{-2}$ state.

The maxima of the distribution (4) for each peak are located in accordance with Eq. (3) and the calculated HF energies of the discrete levels. The cross section σ_0 is expressed through the calculated photoelectron recapture probabilities into the discrete states, $P_{\rm dis}^{(n)}$, as $\sigma_0 = \frac{P_{\rm dis}^{(n)}\,\Gamma_{\rm dis}}{2\pi}$. We can note that according to Eq. (4), both the width and the maximum value of the calculated discrete peaks depend on the value of $\Gamma_{\rm dis}$; with a growth of $\Gamma_{\rm dis}$, the peaks become wider and their heights decrease. The value $\Gamma_{\rm dis} = 236$ meV used in our calculation leads to a satisfactory agreement with the measured widths of the peaks but shows slightly larger peak intensities [see Fig. 4(c)]. This fact can be attributed to the approximate character of the HF discrete wave function used in our approach.

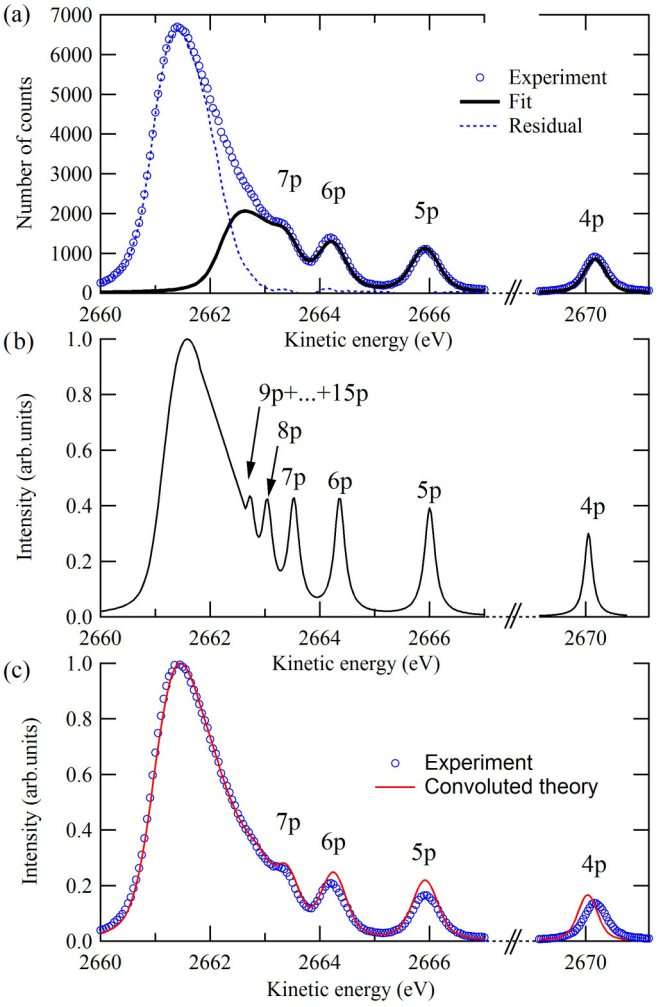

FIG. 4. (Color online) Experimental and calculated Auger spectrum at excess energy $E_{\rm exc} = 1$ eV above the Ar $1s$ ionization threshold. (a) Experimental spectrum (blue circles) with a tentative fit to the individual contributions from discrete Rydberg states (see text for details). (b) Calculated Auger spectrum with recapture to discrete np states with $n = 4$–15. (c) Convoluted theoretical spectrum (see text for details on the convolution) compared to the experimental spectrum (blue circles).

Considering the model used, good agreement between the calculations and the experimental spectrum is obtained, and the sum of the cross sections (4) of the recapture into the $4p$–$15p$ states reproduces well the line shape in the region of the low discrete states. On the other hand, the recapture of a slow photoelectron into high discrete states (with $n > 15$), which are located very dense in the near-threshold region, $0 > E_i > -0.3$ eV, leads to the quasicontinuous energy distribution of the recaptured electrons. It is reasonable to simulate this distribution by the linear function that merges at threshold into the energy distribution of the photoelectrons in continuum. A criterion of validity of such a model is the equality of the integral of the energy distribution of the Auger electrons over all the energies (including both the discrete and continuum parts of the photoelectrons) to the total cross section, $\sigma_{\rm tot}(E_{\rm exc})$ [56].

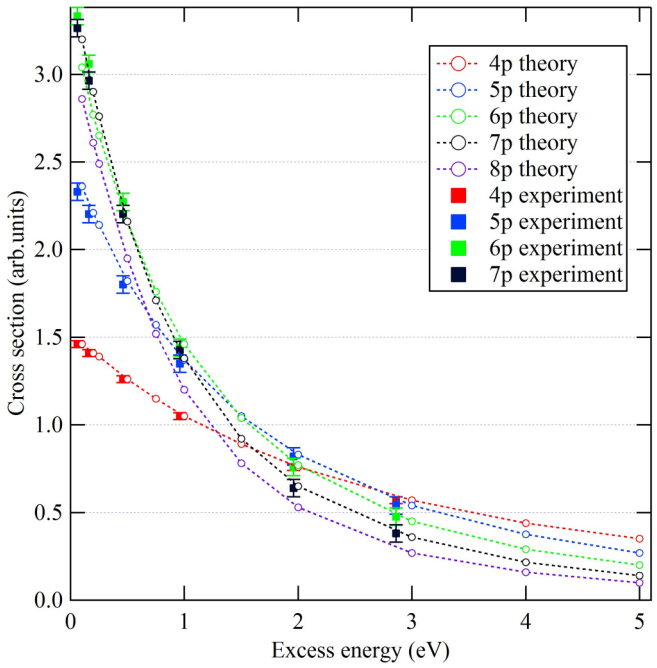

FIG. 5. (Color online) Experimental and calculated individual recapture cross sections for discrete Rydberg states $n = 4$–8 as a function of excess photon energy above the Ar 1*s* ionization threshold.

The energy distribution of the Auger electrons calculated within this approach satisfies this criterion with high accuracy (with a relative error less than 1%). Note that the representation of the discrete states by Eq. (4) is equivalent to the convolution of this part of the Auger spectrum with a Lorentzian of $\Gamma_{\rm dis} = 236$ meV FWHM. As discussed in Sec. II, the continuum part of the Auger spectrum must also be convolved with a Lorentzian of 236 meV FWHM. The result of this convolution is the spectrum shown in Fig. 4(b). Finally, the discrete part has been convoluted with a Gaussian function of 350 meV FWHM to account for the photon bandwidth, and the entire calculated spectrum has been convoluted with a Gaussian function of 300 meV to simulate the electron detector resolution. The convoluted calculated spectrum is compared to the experimental spectrum in Fig. 4(c). It is known that the HF values of the discrete levels do not coincide with the measured ones, and our comparison shows also different but rather close values.

The calculated individual cross sections of the PCI recapture for the discrete states with $n = 4$–8 are presented as a function of excess energy $E_{\rm exc}$ above threshold in Fig. 5, compared to the experimental cross sections with $n = 4$–7. The experimental cross sections were obtained by a least-squares-fitting procedure [shown as a thick black curve in Fig. 4(a)], and they are normalized to the $4p$ theoretical cross section for comparison with the calculated values. Since only the states $n = 4$–7 are resolved in the experimental spectrum, in the fit analysis the relative energy position of the $n = 8$ state was taken from the calculations. This peak described the contributions of all the higher Rydberg states, and it was included in the fit analysis in order to extract tentatively the intensity of the $7p$ state.

We observe that for low excess energy $E_{\rm exc}$ the photoelectron capture occurs mainly in the np states with $n = 5$–8. We also note that the variation of the individual cross sections with excess energy above threshold is state-dependent. The cross section of the higher states ($n = 6$–8) decreases very rapidly with photon energy in the first 3 eV above threshold, where states $n = 6$ and 7 dominate the recapture just above threshold. Above ~3 eV, the photoelectron recapture cross sections into the discrete states decrease monotonically and are ordered in magnitude following the principal quantum number n: $P_{\rm dis}^{(4)} > P_{\rm dis}^{(5)} > P_{\rm dis}^{(6)} > P_{\rm dis}^{(7)} > P_{\rm dis}^{(8)}$. This behavior is due to the overlap of the radial wave function of the emitted photoelectron in the intermediate and final discrete states. According to the general PCI picture, the probability of the PCI recapture into these state decreases with increasing excess energy $E_{\rm exc}$. This result is also in agreement with the results of the investigation of PCI recapture in Ne 1*s* decay [13]. Good agreement between the calculated and measured cross sections is observed, although in the region $E_{\rm exc} < 0.5$ eV the measured values for the capture into the $5p$ and $6p$ states are slightly larger than the calculated ones.

V. CONCLUSION

We have presented in this article a joint experimental and theoretical investigation of PCI effects revealed in the *KLL* Auger decay of argon photoionized above the 1*s* ionization threshold by high-resolution measurements of fast Auger electrons (~2262 eV). The effect of the interaction between the Auger electron, the photoelectron, and the field of the ion is essentially twofold. A strong distortion of the Auger electron's energy distribution is observed as a function of photon energy. In agreement with the general PCI picture, the position of the maximum intensity is shifted in energy by a large positive value close to threshold (~1 eV), i.e., the Auger electron gains energy. This shift decreases with increasing photon energy, and the Auger line reaches a limit value about 150 eV above threshold. The line shape is also strongly affected by PCI. The asymmetry of the Auger line, large close to threshold, decreases with increasing photon energy. The second manifestation of PCI in the energy region close to threshold, $E_{\rm exc} < 3$ eV, is the recapture of the 1*s* photoelectron into discrete Rydberg states above threshold. Our main achievement is to be able to take into account both the continuum part of the Auger decay and the contributions of states $n = 4$ to 15 to the recapture cross sections, i.e., on the large-energy wing, to reproduce with good accuracy the Auger electron energy distribution at low photon energy above threshold, where the PCI effects are the stronger. The good agreement of the measured and calculated spectra confirms the reliability of the model. Our work shows that the investigation of the high-energy Auger spectrum is a powerful method to study PCI effects after deep-shell photoionization. We believe this approach is general and can be applied to the investigation of PCI effects in other atomic and molecular systems.

ACKNOWLEDGMENTS

Experiments were performed on the GALAXIES beamline at SOLEIL Synchrotron, France (Proposal No. 20120122). We are grateful to D. Prieur for technical assistance and to the SOLEIL staff for their smooth operation of the facility.

[1] M. Yu. Kuchiev and S. A. Sheinerman, Sov. Phys. Usp. **32**, 569 (1989).
[2] V. Schmidt, Rep. Prog. Phys. **55**, 1483 (1992).
[3] R. Guillemin, S. Sheinerman, C. Bomme, L. Journel, T. Marin, T. Marchenko, R. K. Kushawaha, N. Trcera, M. N. Piancastelli, and M. Simon, Phys. Rev. Lett. **109**, 013001 (2012).
[4] F. Penent, J. Palaudoux, P. Lablanquie, L. Andric, R. Feifel, and J. H. D. Eland, Phys. Rev. Lett. **95**, 083002 (2005).
[5] J. H. D. Eland, in *Advances in Chemical Physics*, Vol. 141, edited by S. A. Rice (John Wiley & Sons, Inc., Hoboken, NJ, 2009), Chap. 3.
[6] S. Sheinerman, P. Lablanquie, F. Penent, Y. Hikosaka, T. Kaneyasu, E. Shigemasa, and K. Ito, J. Phys. B **43**, 115001 (2010).
[7] F. Penent, S. Sheinerman, L. Andric, P. Lablanquie, J. Palaudoux, U. Becker, M. Braune, J. Viefhaus, and J. H. D. Eland, J. Phys. B **41**, 045002 (2008).
[8] S. Sheinerman, P. Lablanquie, F. Penent, J. Palaudoux, J. H. D. Eland, T. Aoto, Y. Hikosaka, and K. Ito, J. Phys. B **39**, 1017 (2006).
[9] P. Lablanquie, S. Sheinerman, L. Andric, J. Palaudoux, Y. Hikosaka, K. Ito, and F. Penent, J. Electron Spectrosc. Relat. Phenom. **185**, 198 (2012).
[10] S. Sheinerman, P. Linusson, J. H. D. Eland, L. Hedin, E. Andersson, J.-E. Rubensson, L. Karlsson, and R. Feifel, Phys. Rev. A **86**, 022515 (2012).
[11] C. Bomme, R. Guillemin, S. Sheinerman, T. Morin, L. Journel, T. Marchenko, R. K. Kushawaha, N. Trcera, M. N. Piancastelli, and M. Simon, J. Phys. B **46**, 215101 (2013).
[12] H. Aksela, M. Kivilompolo, E. Nõmmiste, and S. Aksela, Phys. Rev. Lett. **79**, 4970 (1997).
[13] U. Hergenhahn, A. De Fanis, G. Prümper, A. K. Kazansky, N. M. Kabachnik, and K. Ueda, J. Phys. B **38**, 2843 (2005).
[14] E. Shigemasa, T. Kaneyasu, Y. Tamenori, and Y. Hikosaka, J. Electron Spectrosc. Relat. Phenom. **156-158**, 289 (2006).
[15] T. Gejo, T. Ikegami, K. Honma, O. Takahashi, E. Shigemasa, Y. Hikosaka, and Y. Tamenori, J. Chem. Phys. **140**, 214310 (2014).
[16] H. Hanashiro, Y. Suzuki, T. Sasaki, A. Mikuni, T. Takayanagi, K. Wakiya, H. Suzuki, A. Danjo, T. Hino, and S. Ohtani, J. Phys. B **12**, L775 (1979).
[17] S. Hedman, K. Helenelund, L. Asplund, U. Gelius, and K. Siegbahn, J. Phys. B **15**, L799 (1982).
[18] K. Helenelund, S. Hedman, L. Asplund, U. Gelius, and K. Siegbahn, Phys. Scr. **27**, 245 (1983).
[19] V. Schmidt, N. Sandner, W. Mehlhorn, M. J. Adam, and F. Wuilleumier, Phys. Rev. Lett. **38**, 63 (1977).
[20] R. Guillemin, C. Bomme, T. Marin, L. Journel, T. Marchenko, R. K. Kushawaha, N. Trcera, M. N. Piancastelli, and M. Simon, Phys. Rev. A **84**, 063425 (2011).
[21] U. Alkemper, J. Doppelfeld, and F. von Busch, Phys. Rev. A **56**, 2741 (1997).
[22] D. Céolin, T. Marchenko, R. Guillemin, L. Journel, R. K. Kushawaha, S. Carniato, S.-M. Huttula, J. P. Rueff, G. B. Armen, M. N. Piancastelli, and M. Simon, Phys. Rev. A **91**, 022502 (2015).
[23] A. Niehaus, J. Phys. B **10**, 1845 (1977).
[24] M. Ya. Amusia, M. Yu. Kuchiev, and S. A. Sheinerman, Sov. Phys. JETP **47**, 238 (1979).
[25] M. Yu. Kuchiev and S. A. Sheinerman, J. Phys. B **18**, L551 (1985).
[26] A. Russek and W. Mehlhorn, J. Phys. B **19**, 911 (1986).
[27] M. Yu. Kuchiev and S. A. Sheinerman, Sov. Phys. JETP **63**, 986 (1986).
[28] F. Koike, J. Phys. B **20**, 1965 (1987).
[29] G. B. Armen, J. Tulkki, T. Aberg, and B. Crasemann, Phys. Rev. A **36**, 5606 (1987).
[30] M. Yu. Kuchiev and S. A. Sheinerman, J. Phys. B **21**, 2027 (1988).
[31] P. van der Straten, R. Morgenstern, and A. Niehaus, Z. Phys. D **8**, 35 (1988).
[32] A. K. Kazansky and N. M. Kabachnik, Phys. Rev. A **72**, 052714 (2005).
[33] L. Gerchikov and S. Sheinerman, Phys. Rev. A **84**, 022503 (2011).
[34] Q. Wang, S. Sheinerman, and F. Robicheaux, J. Phys. B **47**, 215003 (2014).
[35] B. Kämmerling, B. Krässig, and V. Schmidt, J. Phys. B **26**, 261 (1993).
[36] L. Avaldi, P. Belotti, P. Bolognesi, R. Camilloni, and G. Stefani, Phys. Rev. Lett. **75**, 1915 (1995).
[37] N. Scherer, H. Lörch, T. Kerkau, and V. Schmidt, J. Phys. B **37**, L121 (2004).
[38] A. L. Landers, F. Robicheaux, T. Jahnke, M. Schöffler, T. Osipov, J. Titze, S. Y. Lee, H. Adaniya, M. Hertlein, P. Ranitovic, I. Bocharova, D. Akoury, A. Bhandary, T. Weber, M. H. Prior, C. L. Cocke, R. Dörner, and A. Belkacem, Phys. Rev. Lett. **102**, 223001 (2009).
[39] M. O. Krause, J. Phys. Chem. Ref. Data **8**, 307 (1979).
[40] D. V. Morgan, R. J. Bartlett, and M. Sagurton, Phys. Rev. A **51**, 2939 (1995).
[41] J. L. Campbell and T. Papp, At. Data Nucl. Data Tables **77**, 1 (2001).
[42] J. C. Levin and G. B. Armen, Radiat. Phys. Chem. **70**, 105 (2004).
[43] W. Mehlhorn, in *Atomic Inner-shell Physics*, edited by B. Crasemann (Plenum, New York, 1985), p. 119.
[44] V. Schmidt, *Electron Spectroscopy of Atoms Using Synchrotron Radiation* (Cambridge University Press, Cambridge, 1997).
[45] G. B. Armen, H. Aksela, T. Aberg, and S. Aksela, J. Phys. B **33**, R49 (2000).
[46] M. Jurvansuu, A. Kivimäki, and S. Aksela, Phys. Rev. A **64**, 012502 (2001).
[47] J.-P. Rueff, J. M. Ablett, D. Céolin, D. Prieur, Th. Moreno, V. Balédent, B. Lassalle-Kaiser, J. E. Rault, M. Simon, and A. Shukla, J. Synch. Radiat. **22**, 175 (2015).
[48] D. Céolin, J. M. Ablett, D. Prieur, T. Moreno, J.-P. Rueff, T. Marchenko, L. Journel, R. Guillemin, B. Pilette, T. Marin, and M. Simon, J. Electron Spectrosc. Relat. Phenom. **190**, 188 (2013).
[49] M. N. Piancastelli, G. Goldsztejn, T. Marchenko, R. Guillemin, R. K. Kushawaha, L. Journel, S. Carniato, J.-P. Rueff, D. Céolin, and M. Simon, J. Phys. B **47**, 124031 (2014).
[50] M. Simon, R. Püttner, T. Marchenko, R. Guillemin, R. K. Kushawaha, L. Journel, G. Goldsztejn, M. N. Piancastelli, J. M. Ablett, J.-P. Rueff, and D. Céolin, Nat. Commun. **5**, 4069 (2014).
[51] J. A. R. Samson, Rev. Sci. Instrum. **40**, 1174 (1969).
[52] J. C. Levin, C. Biedermann, N. Keller, L. Liljeby, C.-S. O, R. T. Short, I. A. Sellin, and D. W. Lindle, Phys. Rev. Lett. **65**, 988 (1990).

[53] J. Doppelfeld, N. Anders, B. Esser, F. von Busch, H. Scherer, and S. Zinz, J. Phys. B **26**, 445 (1993).

[54] L. Asplund, P. Kelfve, B. Blomster, H. Siegbahn, and K. Siegbahn, Phys. Scr. **16**, 268 (1977).

[55] M. Yu. Kuchiev and S. A. Sheinerman, Comput. Phys. Commun. **39**, 155 (1986).

[56] S. A. Sheinerman, J. Phys. B **36**, 4435 (2003).